APPLICATION OF THE FINITE ELEMENT METHOD TO DETERMINE THE VELOCITY PROFILE IN AN OPEN CHANNEL

Daria Wotzka
Faculty of Electrical Engineering, Automatic Control and Informatics
Opole University of Technology
ul. Prószkowska 76
45-758 Opole, Poland
E-mail: d.wotzka@po.edu.pl

KEYWORDS
Finite element methods, laminar flow, turbulent flow, open channel

ABSTRACT

This paper contains the results of work on the simulation of laminar and turbulent flows using the finite element method. In particular, exemplary literature references are indicated, boundary and initial conditions are described, and numerical results are illustrated, including fluid velocity distributions and profiles in a cylindrical open channel structure.

INTRODUCTION

Urban and rural development, caused by a constant increase in the number of inhabitants, results in an increase in the amount of sewage which flows into the central sanitary sewer infrastructure. While the construction of new housing developments is associated with the simultaneous construction of sanitary sewers with an appropriately sized volume, in some inner-city areas it is not physically or economically feasible to extend existing sewers, usually open channels, which are currently operating often at the limit of their capacity.

Improving the monitoring system of sanitary networks is now an important industry to assess its hydraulic performance. The main problem faced by water and sewerage companies concerns the systematic collection of, among others, the volume and velocity of sewage flow in open sewers (Synowiecka *et al.*, 2014) and the thickness of sewer sludge in overflow collectors (Kalinowski, 2016). Lack of supervision over the proper operation of the sewage disposal system may cause leakage, resulting in a potential threat to life and health of the region's inhabitants and environmental contamination. The access to the current parameters of the system operation enables the estimation of the load in particular areas and the detection of undesirable phenomena, such as the occurrence of ponding and flaring in the canal or exceeding of maximum fills (Synowiecka *et al.*, 2014).

One of the areas of current scientific and research work is the construction of simulation models of sanitary systems, which can be used to predict the behaviour of networks under different operating conditions. The values of sewage system operating parameters, which are recorded on a regular basis, constitute an important and necessary element of the process of calibration and validation of mathematical models.

The phenomenon of fluid flow in sewers has been described in detail to some extent in the literature. Equations and mathematical models characterizing the flow through channels of different shapes, such as trapezoid, rectangle or cylinder, have been indicated (Chow, 1988; Jobson and Froehlich, 1988; Sturm, 2001; Basu, 2019a, 2019b). However, sewerage systems, especially in large agglomerations are diverse, consisting of channels of different sizes and shapes with numerous crossing points. In Poland, many water and sewerage companies do not yet have metering systems for wastewater or rainwater infrastructure. Measurement of linear velocity of flow in successive network sections is still a technological challenge and an important element of development of existing sewage infrastructure. The problem in question arises from the necessity of installing the measuring device usually in very polluted canals, in a possibly non-invasive way, not causing any disturbances in the proper flow of waste water.

The main objective of the conducted scientific and research work is to develop a device for measuring the volume flow rate in the sewage system, which has an implementation potential (Wotzka, 2022). In particular, the device should meet the condition of possibly low invasiveness in the normal flow of sewage in an open sewer. An additional constraint is the condition of low production cost of the developed device. It has been proposed that ultrasonic acoustic signals be used to determine the velocity using a cross-correlation method. The cross-correlation method allows the calculation of the linear velocity of particles moving inside an open channel. To calculate the flow rate, it is necessary to know the area A through which the fluid flows. In order to determine the velocity profile in the different layers of a cylindrical open channel, a computer model was developed and a series of simulations were performed as part of the research

Communications of the ECMS, Volume 36, Issue 1,
Proceedings, ©ECMS Ibrahim A. Hameed, Agus Hasan,
Saleh Abdel-Afou Alaliyat (Editors) 2022
ISBN: 978-3-937436-77-7/978-3-937436-76-0(CD) ISSN 2522-2414

work. The model was made in COMSOL Multiphysics environment using the CFD module, which uses algorithms based on the finite element method (FEM) to approximate solutions of partial differential equations.
The scope of the conducted research included the analysis of the influence of the following model parameters on the obtained velocity distributions:
- fluid level H={0.05; 0.09; 0.12} m in the channel,
- channel length L={1; 10} m,
- object input velocity v={0.2; 0.3} m/s.
In the following sections of the paper the numerical method used and the simulation results obtained are presented.

NUMERICAL METHOD IN OPEN CHANNEL FLOW STUDIES

Numerical methods are now an important alternative to experimental studies due, among other things, to the high-powered computing computers available today and a number of software solutions that offer a relatively affordable application of the CFD method (Ramanathan, 2013; Lai and Kuowei Wu, 2019).
One of the areas of application of numerical methods is the study of changes in the geometry of river currents occurring during floods, particularly near bridges (Adhikary, Majumdar and Kostic, 2009) and studies of sediment transport modeling (Nations, no date; *Hydrology and Sediment Transport.*, 2010; Lai and Kuowei Wu, 2019). Another area of research is work related to hydraulic structures, which includes channel widening which provides a transition from a narrow to a relatively wide channel cross-section (Najmeddin, 2012). At the transition point, the flow tends to separate from the spreading sidewalls and forms turbulent vortices when the divergence angle exceeds a threshold value. This phenomenon can cause unwanted flow energy loss and sidewall erosion. The author of (Najmeddin, 2012) presented the results of a study on adjusting the lift in the vertical plane to eliminate flow separation. He used CFD modeling in this study, which allowed a systematic investigation of the effects of different divergence angles, lift heights and Froude number for subcritical flow. The modeling results were validated using analytical solutions under simplified conditions and available experimental data for a limited number of cases.
Another issue investigated is the occurrence of arcs in both natural and artificial open channels. Due to the change in pressure and centrifugal force values, as well as the interaction between these two forces, strong secondary flows are generated in the bends of open channels, which in turn cause a full three-dimensional complex fluid flow in the area where the channel bends. Many numerical studies have been conducted to model the characteristics of open channel bends. For example, the author of (Gholami *et al.*, 2015) used CFD methods to study the flow depth and velocity field in acute angle bends, including considering two phases water and air.
On the other hand, in the paper (Gandhi, Verma and Abraham, 2010) the authors used CFD method to study the flow velocity profile in rectangular open channels for determining the optimal number and location of flow sensors.

BOUNDARY AND INITIAL CONDITIONS IN THE NUMERICAL MODEL

The test object is a cylinder filled with liquid up to a certain height H, flowing along the object with a constant average velocity v, determined at the surface of the inlet opening. In the considered modeling task using the FEM method, the Navier-Stokes equations are solved under laminar (1-2) and turbulent (2-5), incompressible fluid flow conditions. The dependent variables in the model are the field components of velocity u, v, w and pressure p. In the task, a constant temperature T=293.15 K and zero initial conditions: u=(0,0,0) m/s, p=0 Pa were assumed.

$$\rho(\mathbf{u}\cdot\nabla)\mathbf{u} = \nabla\cdot[-p\mathbf{I} + \mu(\nabla\mathbf{u} + (\nabla\mathbf{u})^{\mathbf{T}})] + \mathbf{F}, \quad (1)$$

where: $\mathbf{u}$ – velocity vector, ρ – density, p – pressure, μ – dynamic viscosity, $\mathbf{F}$ – volumetric force vector, $\mathbf{I}$ – intensity vector.

$$\rho\nabla\cdot(\mathbf{u}) = 0, \quad (2)$$

$$\rho(\mathbf{u}\cdot\nabla)\mathbf{u} = \nabla\cdot[-p\mathbf{I} + (\mu + \mu_{\mathrm{T}})(\nabla\mathbf{u} + (\nabla\mathbf{u})^{\mathbf{T}})] + \mathbf{F}, \quad (3)$$

where: μ_{T} – dynamic viscosity of the turbulent model $k-\epsilon$.

$$\rho(\mathbf{u}\cdot\nabla)k = \nabla\cdot\left[\left(\mu + \frac{\mu_{\mathrm{T}}}{\sigma_{\mathrm{k}}}\right)\nabla k\right] + p_k - \rho\epsilon, \quad (4)$$

where: k=5.202·10^{-7} m^2/s^3, kinetic energy, ϵ=2.412·10^{-9} m^2/s^3 dispersion coefficient, σ_{k}=1 turbulent model parameter, p_k - A component of the turbulent kinetic energy source.

$$\rho(\mathbf{u}\cdot\nabla)\epsilon = \nabla\cdot\left[\left(\mu + \frac{\mu_{\mathrm{T}}}{\sigma_{\epsilon}}\right)\nabla\epsilon\right] + c_{\epsilon 1}\frac{\epsilon}{k}p_k - c_{\epsilon 2}\rho\frac{\epsilon^2}{k}, \quad (5)$$

where: σ_{ϵ}=1.3, $c_{\epsilon 1}$=1.44, $c_{\epsilon 2}$=1.92 are the parameters of the turbulent model.

$$\mu_{\mathrm{T}} = c_{\mu}\rho\frac{k^2}{\epsilon}, \quad (6)$$

$$p_k = \mu_{\mathrm{T}}[\nabla\mathbf{u}:\nabla\mathbf{u} + (\nabla\mathbf{u})^{\mathbf{T}}], \quad (7)$$

where: c_{μ}=0.09 is a turbulent model parameter.

Fig. 1-3 depict a visualization of the object along with the boundary conditions B1-B4. The following boundary conditions were assumed in the task.

Boundary condition B1 - non-slip fixed wall Laminar flow is calculated assuming $\mathbf{u} = 0$. Turbulent flow is calculated with (8-11).

$$\mathbf{u} \cdot \mathbf{n} = 0, \tag{8}$$

$$[(\mu + \mu_{\mathrm{T}})(\nabla\mathbf{u} + (\nabla\mathbf{u})^{\mathbf{T}})]\mathbf{n} = \rho\frac{u_\tau}{u^+}\mathbf{u}_{\mathrm{tang}}, \tag{9}$$

$$\mathbf{u}_{\mathrm{tang}} = \mathbf{u} - (\mathbf{u} \cdot \mathbf{n})\mathbf{n}, \tag{10}$$

$$\nabla k \cdot \mathbf{n} = 0, \epsilon = \rho\frac{c_\mu k^2}{\varkappa_v \delta_w^+ \mu}, \tag{11}$$

where: $\mathbf{n}$ – normal vector, u_τ – tangential speed, u^+– friction speed, $\varkappa_v$=0.41, δ_w^+=0.2 are the parameters of the turbulent model.

The wall condition applies to fluid flow with stationary walls. No-slip is the default boundary condition for modeling solid walls. A no-slip wall is one in which the fluid velocity relative to the wall velocity is zero.

Boundary condition B2 - open edge with normal stress f_0=0 N/m^2. Laminar flow is calculated with (12). Turbulent flow is calculated with (13-14).

$$[-p\mathbf{I} + \mu(\nabla\mathbf{u} + (\nabla\mathbf{u})^{\mathbf{T}})]\mathbf{n} = -f_0\mathbf{n}, \tag{12}$$

$$[-p\mathbf{I} + (\mu + \mu_{\mathrm{T}})(\nabla\mathbf{u} + (\nabla\mathbf{u})^{\mathbf{T}})]\mathbf{n} = f_0\mathbf{n}, \tag{13}$$

$$\begin{cases} \nabla k \cdot \mathbf{n} = 0, \nabla\epsilon \cdot \mathbf{n} = 0, \\ \quad if\ \mathbf{u} \cdot \mathbf{n} \geq 0, \\ k = \dfrac{3}{2}(U_{\mathrm{ref}} I_{\mathrm{T}})^2, \epsilon = c_\mu^{\frac{3}{4}}\dfrac{k^{\frac{3}{2}}}{L_{\mathrm{T}}} \\ \quad if\ \mathbf{u} \cdot \mathbf{n} < 0. \end{cases} \tag{14}$$

where: U_{ref} – reference speed, I_{T} – intensity, L_{T} – length are the scale parameters of the turbulent model.

The open edge condition describes the boundaries of the domain that are in contact with a large volume of fluid that can both flow into and out of the domain beyond the object region. The normal stress condition f_0 means that $f_0 \approx p$.

Boundary condition B3 - constant pressure with backflow suppression p_0=0, $\hat{p}_0 \leq p_0$. Laminar flow is calculated with (15). Turbulent flow is calculated with (16-17). This condition is applicable at boundaries for which there is outflow from the domain. In order to obtain a proper numerical solution, it is recommended to consider the inlet conditions when determining the outlet condition. For example, if velocity is specified at the inlet, pressure can be specified at the outlet and vice versa.

$$[-p\mathbf{I} + \mu(\nabla\mathbf{u} + (\nabla\mathbf{u})^{\mathbf{T}})]\mathbf{n} = -\hat{p}_0\mathbf{n}, \tag{15}$$

$$[-p\mathbf{I} + (\mu + \mu_{\mathrm{T}})(\nabla\mathbf{u} + (\nabla\mathbf{u})^{\mathbf{T}})]\mathbf{n} = -\hat{p}_0\mathbf{n}, \tag{16}$$

$$\nabla k \cdot \mathbf{n} = 0, \nabla\epsilon \cdot \mathbf{n} = 0, \tag{17}$$

Specifying the velocity vector at both the inlet and the outlet can cause convergence problems. Selecting the appropriate outlet conditions for the Navier-Stokes equations is a non-trivial task. This option determines the normal stress, which in most cases is approximately equal to the pressure. The tangential component of the stress equals zero. If the reference pressure p_{ref} is 0, then the pressure p_0 t the domain boundary is the absolute pressure. Otherwise p_0 is the relative pressure at the boundary.

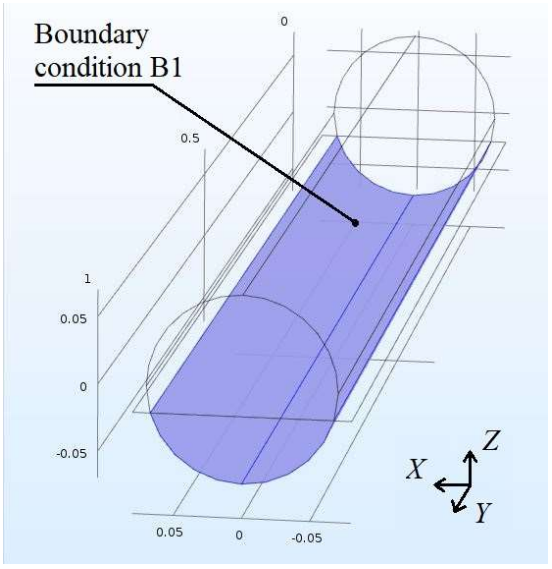

Fig. 1 Visualization of the boundary condition B1.

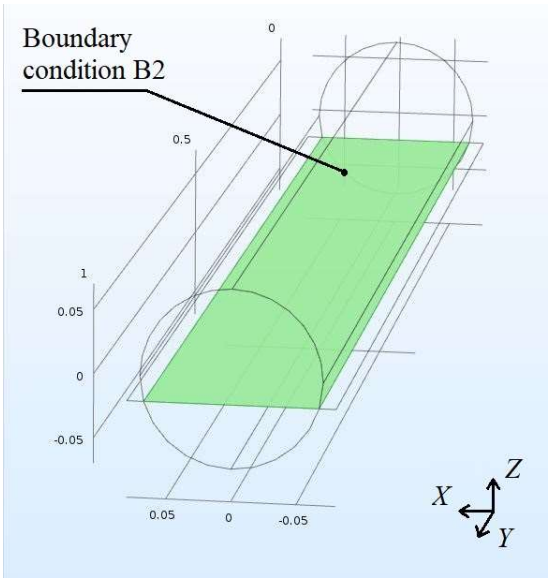

Fig. 2 Visualization of the boundary condition B2.

Boundary condition B4 - normal inlet speed U_0=0.2 m/s, $\mathbf{u} = -U_0\,\mathbf{n}$, where $\mathbf{n}$ is the boundary normal directed out of the area, and, a U_0 is the normal inflow velocity, $U_{\text{ref}} = U_0$, $k = (U_{\text{ref}} I_{\text{T}})^2$, $\epsilon = \frac{k^{3/2}}{L_{\text{T}}}$.

This condition is applicable at boundaries for which there is a net flow to the interior of the domain. In addition, the following other parameters are specified in the task:
- reference temperature T_{ref} = 293.15 K,
- reference pressure level p_{ref} = 1 atm,
- absolute pressure $p_{\text{bw}} = p$ [Pa] + p_{ref},
- speed value U [m/s] calculated as $U = \sqrt{(u)^2 + (v)^2 + (w)^2}$, where *u, v, w* are the dependent variables computed by the numerical method in the domain under consideration.

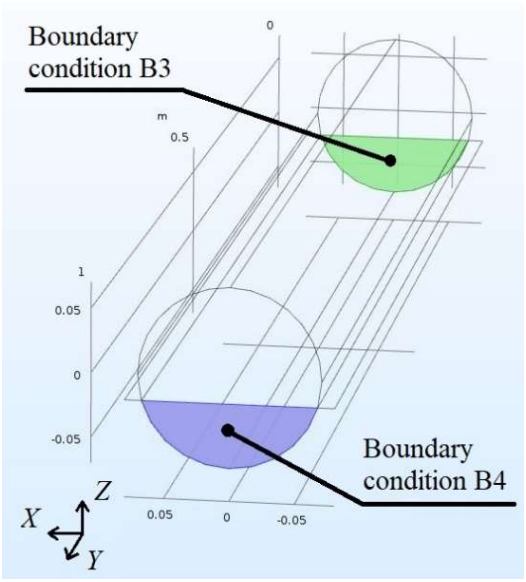

Fig. 3 Visualization of boundary conditions B3 and B4.

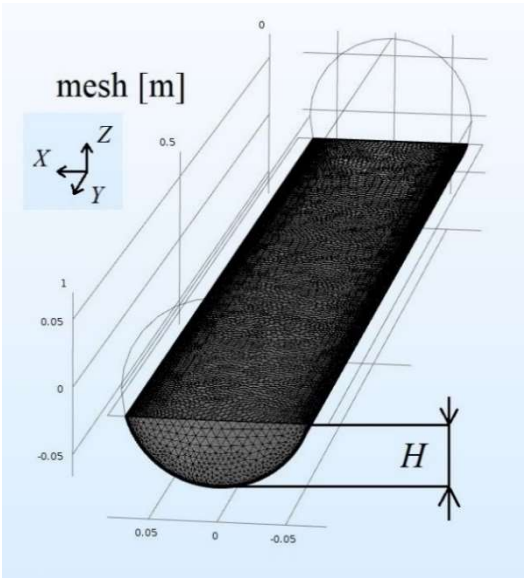

Fig. 4 Visualization of the discretization mesh used in the numerical model.

Table 1 lists the values of the discretization mesh parameters used in the numerical model. A visualization of the grid elements is shown in Fig. 4.

Table. 1 Parameters used to discretize the object into finite elements.

Description of grid statistics	Value
Minimum element quality	120.6 mm
Average component quality	690.4 mm
Maximum element size	7.9 mm
Minimum element size	1.5 mm
Maximum element growth rate	1.13

The simulation study used a Windows 10 computer with an Intel® Core™ i7-5960X CPU@3.00 GHz, with eight cores. A RAM size of 32 GB was used. The computation time of each simulation depended on the size of the object and ranged from a few minutes to several hours. The FEA algorithms used were Smoothed Aggregation AMG and PARDISO, which are implemented in the COMSOL Multiphysics environment.

RESULTS OF NUMERICAL CALCULATIONS

Fig. 5 illustrates the position of the lines parallel to the ground and with respect to the Y axis, for which the values of the fluid velocity inside the object are visualized in the following section. In particular, these are the positions with respect to the Z-axis: *Z*=0, *Z*=-0.02, *Z*=-0.05 m, which correspond to different heights for the example model, with liquid level in the channel H=0.09 m. Fig. 6 illustrates the position of the lines perpendicular to the bottom and relative to the Y axis. The following section visualizes the liquid velocity values calculated at the positions, which are labeled in Fig. 6 as: Location A - near the liquid outlet, Location B - center of the area, Location C - near the liquid inlet to the object.
In Fig. 7-10, surface distributions of fluid velocity inside a channel of length *d*=1 m and diameter ϕ=0.15 m are illustrated along with isotopes. Fig. 7, 9 and 10 show the results for laminar flow, Fig. 8 shows the results for turbulent flow. The flow velocity in each case was v_{wlot}=0.2 m/s. The liquid level for the results illustrated in Figs. 7 and 8 was *H*=0.12 m, in Fig. 9 the liquid level was *H*=0.09 m, in Fig. 10 the liquid level was *H*=0.05 m.
The lines forming the flow profile are visible in the individual images. Characteristic areas are shaped differently in the inlet area (location C), in the center (location B) as well as in the fluid outlet area from the domain (location A). Slight differences between laminar and turbulent flow can also be seen at the boundary with the wall.

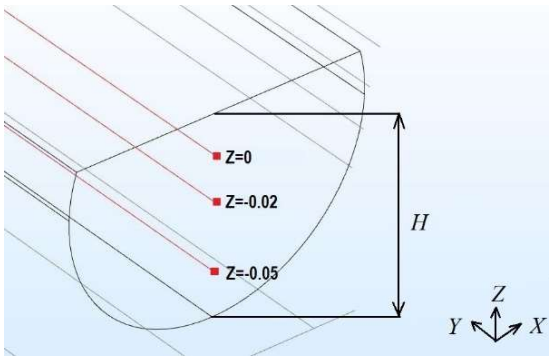

Fig. 5 Visualization of position of the lines on the Z axis parallel to the ground for which the calculation results are illustrated. Model assumes a liquid level of H=0.09 m.

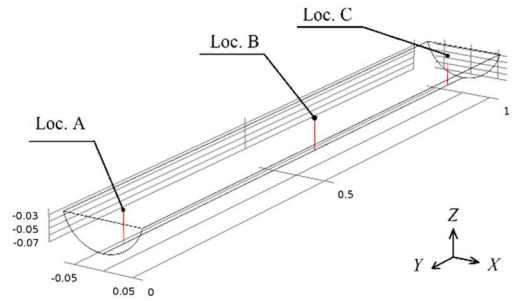

Fig. 6 Visualization of lines perpendicular to the ground of the lines on the Y-axis for which the calculation results were visualized. Liquid level of H=0.05 m was assumed.

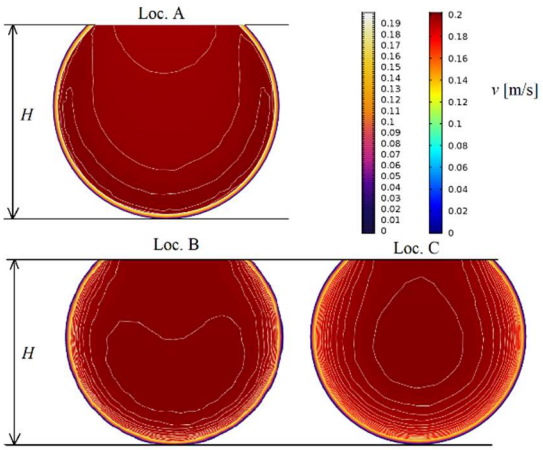

Fig. 7 Surface distributions of fluid velocities inside a channel with length L=1 m and diameter ϕ=0.15 m, fluid height H=0.12 m and assumed laminar flow v_{wlot}=0.2 m/s, at locations A, B and C, as shown in Fig. 6.

Figs. 11-13 illustrate the fluid velocity distributions along a channel ϕ=0.15 m in diameter filled with fluid of height H=0.12 m. Fig. 11 shows the results for a channel of length L=10 m, and Figs. 12 and 13, for a channel of length L=1 m. The presented curves illustrate the change in velocity at different positions relative to the fluid height H, denoted by Z in Fig. 5.

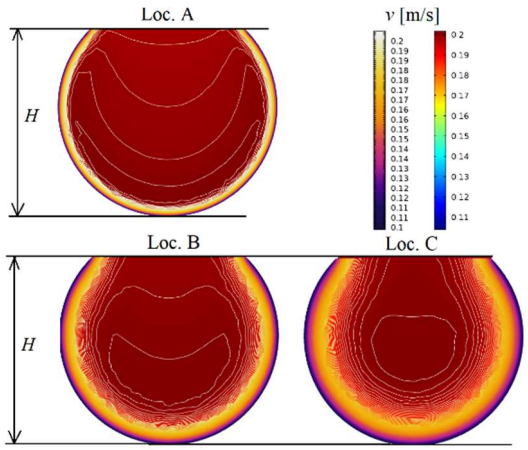

Fig. 8 Surface distributions of fluid velocities inside a channel with length L=1 m and diameter ϕ=0.15 m, fluid height H=0.12 m and assumed turbulent flow v_{wlot}=0.2 m/s, at locations A, B and C, as shown in Fig. 6.

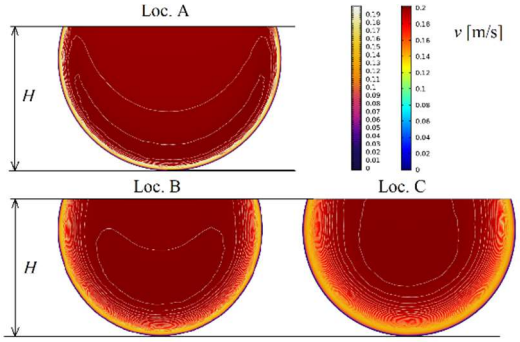

Fig. 9 Surface distributions of fluid velocities inside a channel with length L=1 m and diameter ϕ=0.15 m, fluid height H=0.09 m and assumed laminar flow v_{wlot}=0.2 m/s, at locations A, B and C, as shown in Fig. 6.

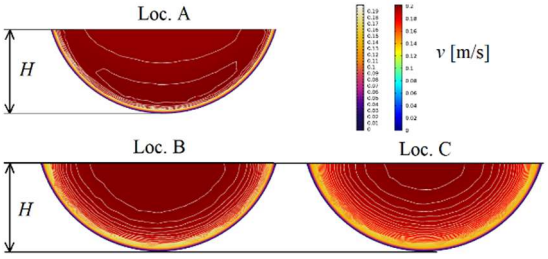

Fig. 10 Surface distributions of fluid velocities inside a channel with length L=1 m and diameter ϕ=0.15 m, fluid height H=0.05 m and assumed laminar flow v_{wlot}=0.2 m/s, at locations A, B and C, as shown in Fig. 6.

The flow velocity at the model inlet was v_{wlot}=0.2 m/s each time. Figs. 11 and 12 show the results for laminar flow, Fig. 13 for turbulent flow. The Figures show decreases in the initial velocity, equal to v_{wlot}=0.2 m/s at the entrance, to 0.18 m/s at the exit for the object with L=10 m, to 0.195 m/s for the object with L=1 m and laminar flow, and to 0.193 m/s for turbulent flow.

Figs. 14-16 illustrate the velocity distributions of the fluid across the channel with a diameter ϕ=0.15 m. The flow velocity at the model inlet was v_{wlot}=0.2 m/s each time. Figs. 14 and 15 show the results for a fluid-filled channel with height H=0.12 m, for laminar and turbulent flow, respectively. In Fig. 16, the results are illustrated for laminar flow in a liquid-filled object up to a height of H=0.05 m.

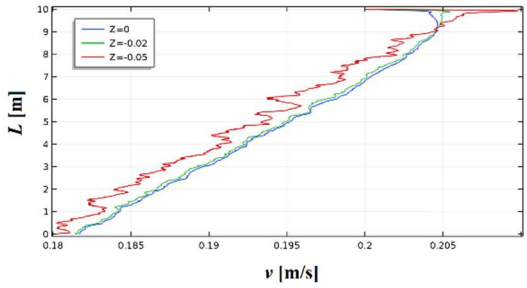

Fig. 11 Laminar flow velocity distribution along the channel of length L=10 m and diameter ϕ=0,15 m, water level H=0,12 m and assumed flow value v_{wlot}=0,2 m/s. The positions correspond to Z marked letter in Fig. 5.

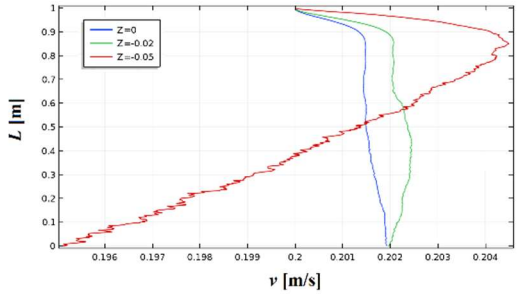

Fig. 12 Laminar flow velocity distribution along the channel with length L=1 m and diameter ϕ=0,15 m, water level H=0,12 m and assumed flow value v_{wlot}=0,2 m/s. The positions correspond to Z marked letter in Fig. 5.

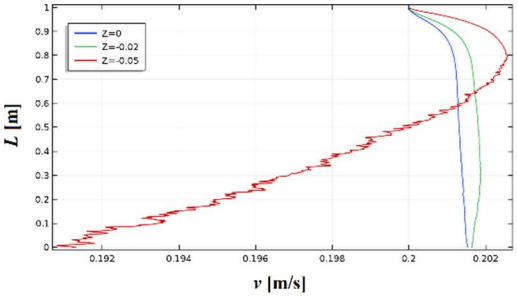

Fig. 13 Turbulent flow velocity distribution along the channel with length L=1 m and diameter ϕ=0,15 m, water level H=0,12 m and assumed flow value v_{wlot}=0,2 m/s. The positions correspond to Z marked letter in Fig. 5.

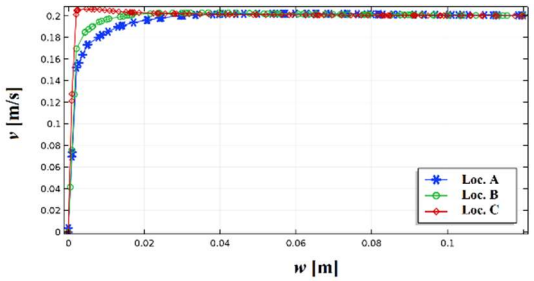

Fig. 14 Laminar flow velocity distribution across the channel of diameter ϕ=0,15 m, water level H=0,12 m and assumed flow value v_{wlot}=0,2 m/s. The positions correspond to A, B, C in Fig. 6.

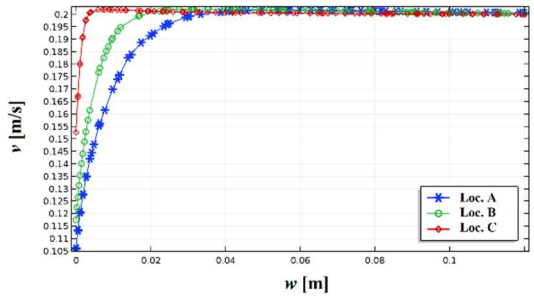

Fig. 15 Turbulent flow velocity distribution across the channel of diameter ϕ=0,15 m, water level H=0,12 m and assumed flow value v_{wlot}=0,2 m/s. The positions correspond to A, B, C in Fig. 6.

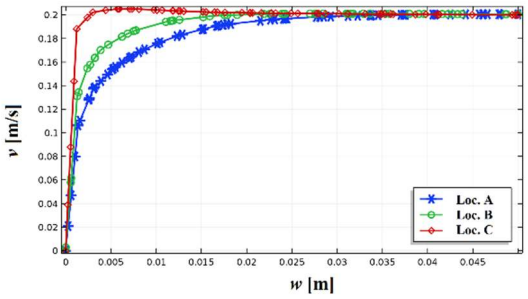

Fig. 16 Laminar flow velocity distribution across the channel of diameter ϕ=0,15 m, water level H=0,05 m and assumed flow value v_{wlot}=0,2 m/s. The positions correspond to these marked with the A, B, C in Fig. 6.

Fig. 17 shows the velocity distribution along a channel with length L=10 m and diameter ϕ=0.15 m, water level H=0.12 m and assumed flow rate v_{wlot}=0.3 m/s as a horizontal plot. The velocity line contours depict velocity gradients, irrelevant inside the channel and significant at the channel walls.
Fig. 18 shows the velocity distribution along the channel with the same parameters as a slice plot.

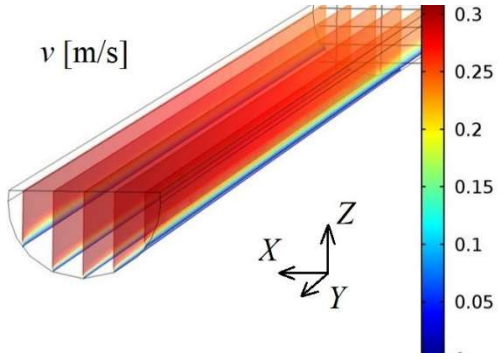

Fig. 18 Velocity distribution along the channel of length L=10 m, diameter ϕ=0.15 m, water level H=0.09 m and assumed flow rate v_{wlot}=0.3 m/s as a slice plot.

CONCLUSIONS

This paper presents the results of the CFD theoretical analyses performed, which involved computer simulations using the FEM method.

As a result of the numerical calculations carried out in the simulation model, velocity profiles were determined in channels with different diameters and levels of their liquid filling and with different lengths. Moreover, the influence of the input velocity on the obtained velocity distributions in particular locations of the considered area was investigated.

Based on the analysis of the obtained relations, it was found that the individual velocity layers can be approximated by circles of increasing diameters and it was assumed that the area A can be approximated by the relation (18). With height h as the input variable, measured by the device under development, and radius r as the input variable, measured independently.

$$A = \frac{1}{2}r^2\left(2\cos^{-1}\left(\frac{r-h}{r}\right) - \sin\left(2\cos^{-1}\left(\frac{r-h}{r}\right)\right)\right), \quad (18)$$

where: A – the area of a segment of a circle of radius r and height h.

The results of the discussed simulation studies confirm the theoretical assumptions made for the development of the measuring device, and equation (18) can be used to calculate the flow velocity in the measuring device mounted in an open channel.

REFERENCES

Adhikary, B. D., Majumdar, P. and Kostic, M. (2009) 'CFD simulation of open channel flooding flows and scouring around bridge structures', in *Proceedings of the 6th WSEAS International Conference on Fluid Mechanics*, pp. 106–113.

Basu, S. (2019a) 'Chapter V - Velocity and Force Type Flow Meter', in Basu, S. (ed.) *Plant Flow Measurement and Control Handbook*. Elsevier, pp. 395–539. doi: 10.1016/b978-0-12-812437-6.00005-6.

Basu, S. (2019b) 'Open channel flow measurement.', in *Plant Flow Measurement and Control Handbook. Fluid, Solid, Slurry and Multiphase Flow. Chapter III*, pp. 257–331. doi: 10.1016/B978-0-12-812437-6.00003-2.

Chow, V. Te (1988) *Open Channel Hydraulics*. McGraw-Hill Book Companny. doi: 10.1016/B978-0-7506-6857-6.X5000-0.

Gandhi, B. K., Verma, H. K. and Abraham, B. (2010) 'Investigation of flow profile in open channels using CFD', in *IGHM*. IIT Roorkee, India, pp. 243–251.

Gholami, A. *et al.* (2015) 'Simulation of open channel bend characteristics using computational fluid dynamics and artificial neural networks', *Engineering Applications of Computational Fluid Mechanics*, 9(1), pp. 355–369. doi: 10.1080/19942060.2015.1033808.

Hydrology and Sediment Transport. (2010). doi: 10.1007/698_2010_67.

Jobson, H. E. and Froehlich, D. C. (1988) *Basic hydraulic principles of open-channel flow*, *U.S. GEOLOGICAL SURVEY, Report 88-707*.

Kalinowski, M. (2016) 'Problemy Monitoringu Przepływu Ścieków I Miąższości Osadów W Przełazowych Kolektorach', *Journal of Civil Engineering, Environment and Architecture*, 63(22), pp. 149–164. doi: 10.7862/rb.2016.156.

Lai, Y. G. and Kuowei Wu (2019) 'A three-dimensional flow and sediment transport model for free-surface open channel flows on unstructured flexible meshes', *Fluids*, 18(4), pp. 1–19. doi: 10.3390/fluids4010018.

Najmeddin, S. (2012) *CFD Modelling of Turbulent Flow in Open-Channel Expansions*. Concordia University.

Nations, F. and A. O. of the U. (no date) *Data Requirements for Sediment Transport Models of Rivers*.

Ramanathan, V. (2013) *Applications of Computational Fluid Dynamics for River Simulation : State of the Practice*.

Sturm, T. (2001) *Open hydraulics channel*. McGraw-Hill Book Companny.

Synowiecka, J. *et al.* (2014) 'Pomiary na czynnych sieciach kanalizacji deszczowej i ogólnospławnej', *Inżynieria Ekologiczna*, 39, pp. 187–197. doi: 10.12912/2081139X.62.

Wotzka, D. (2022) *Koncepcja, wykonanie i badania urządzenia do pomiaru strumienia objętości ścieków w kanale otwartym*. SIM z. 568. OW Politechnika Opolska.

AUTHOR BIOGRAPHIE

DARIA WOTZKA received the M.Sc. degree in Computer Science from the Technische Universität Berlin, Germany and the Ph.D. degree in Electrical Engineering from the Opole University of Technology, Poland. She is a lecturer and research fellow at the Opole University of Technology, Poland. Her research interests include data mining, modeling and simulation applied in engineering and medicine.